# Developing a keV Electron Diode Source

Dean's Research Award – Winter 2026

Luke Concini

April $10^{\text{th}}$, 2026

Supervisor: Dr. Robert Fedosejevs
Graduate Student Mentors: Caleb Guthrie, John Matthew Gjevre

**Abstract**

In this project, we seek to design and produce a keV electron diode source to produce high energy particles used for space sensor calibration. We will investigate the optimal diode geometry to create straight electron trajectories and show that a flat cathode produces the most collimated beam. We will implement high-voltage circuitry via a Cockcroft-Walton generator to drive our diode. Theoretical modelling and experimental refinement will allow us to navigate electric breakdown in our high-voltage vacuum setup. This includes discussion of Paschen breakdown and field emission, and how these arcing methods are exacerbated by diode surface condition and outgassing of plastics in the vacuum chamber. Finally, we will present results from our final test, showing strong evidence of semi-collimated high energy particle production. Reflecting on our results, we will highlight the main areas of improvement, notably marking strategies to improve beam collimation and particle selectivity, as well as increasing the maximum energy of the electrons.

CONTENTS

## I. Introduction

This project involves the design and development of a $keV$ electron source to generate high energy electrons. These electrons will be used to calibrate high-energy electron detectors to be used on a space satellite research mission.

The RADICALS satellite mission, headed by Dr. Ian Mann and in conjunction with numerous Canadian universities, will study the impact of space radiation on Earth's climate. To calibrate these detectors, we need an 'electron gun,' or electron diode source, which can reliably fire electrons with energies in the thousands of electron volts, or $keV$ range. Accurate calibration of these detectors for measurements of high-energy particles near Earth supports this research by improving the quality of data collected.

The implementation of this device must consider challenges involved with high-voltage operation, precision, and measurement, as well as manufacturability. We will investigate the optimal diode geometry to reliably fire electrons along a straight path. We will practically implement our design, including constructing a Cockcroft-Walton voltage multiplier, and an apparatus to withstand high-voltage vacuum conditions. Then, we will use theory to mitigate the likelihood of dielectric breakdown in our high-voltage setup, and iteratively test under vacuum conditions to refine our design. Finally, we will cover our final design, testing, and findings.

## II. FEMM Particle Simulation

We seek to design a diode capable of accelerating electrons across a parallel-plate capacitor device and ejecting them through the anode to be used as a source of high-energy particles. This goal requires a diode capable of liberating electrons at the cathode that will traverse the capacitor and follow a predictable path towards the anode to reliably produce radiation. To accomplish this, we simulated the electric field produced by different capacitor geometries, as well as the electron trajectories that they would produce, to aid in selecting a design. The effectiveness of each option will be judged by field uniformity, impact on the energy of accelerated electrons, and manufacturability.

### A. FEMM Electrostatic Solver

We used an electrostatics solver to obtain the electric field generated by various capacitor geometries along a radial slice of a cylindrically symmetric capacitor. Based on the results of particle trajectory simulations discussed later, we revisited our design and re-simulated different options until we achieved a focused beam of electrons passing through the anode, with minimal divergence.

*1) Methods and Results:* We used the electrostatic solving capabilities of Finite Element Method Magnetics (FEMM) to model the fields produced by various cathode geometries. We varied parameters such as the geometry of the emitter surface from which electrons would be liberated, or the size of the anode hole from which they will exit. To quantify the quality of a given geometry, we used the numerically solved electric field for a given geometry to simulate the trajectories of photoelectrons liberated around the center of the diode. Geometries were considered optimal if they produced a high number of electrons escaping the anode along a straight path.

We took advantage of FEMM's native Lua 4.0 integration to automate the design and analysis of different geometries. We also used the scripting capabilities to automatically export the field data in a regularly sampled grid to our simulation program.

Our first designs incorporated a protruding 'emitter' from the cathode. We experimented with rounded and squared corners, as well as different anode hole geometries, but we consistently found that the elevated emitter resulted in incorrigible divergence of the electron beam from the central axis. The divergence of the electric field around the emitter is seen in Figure 1.

We found that a flat, or planar cathode geometry resulted a uniform field to a very good approximation, allowing electrons to be accelerated orthogonal to the emission surface. This is demonstrated in Figure 2. While there was still some field divergence at the anode hole, the electrons would be moving quickly enough by this point to pass through the diode relatively unhindered.

In general, we found that edge effects around the outside of the capacitor did not affect

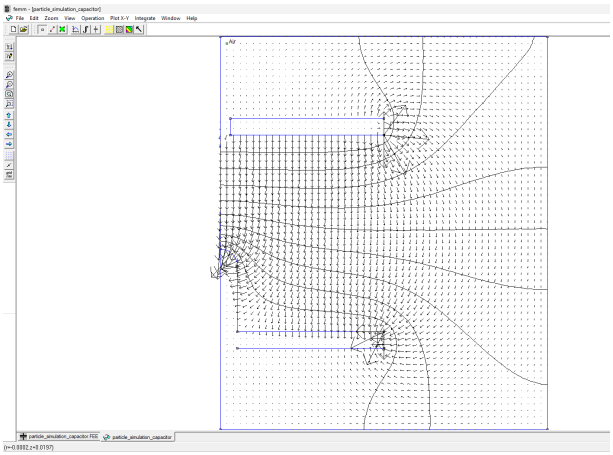

Fig. 1. A combined equipotential contour map and electric field vector plot of the simulated electric field produced by a capacitor with a rounded protrusion. Blue lines represent boundary-condition surfaces, such as metal held at a specific voltage or simulation boundaries. The cathode (bottom) is at a large negative voltage with respect to the grounded anode (top rectangle). This visualization output of a radial slice from FEMM can be coordinated with a Lua script to systematically extract the point-wise data of the solved field for external use.

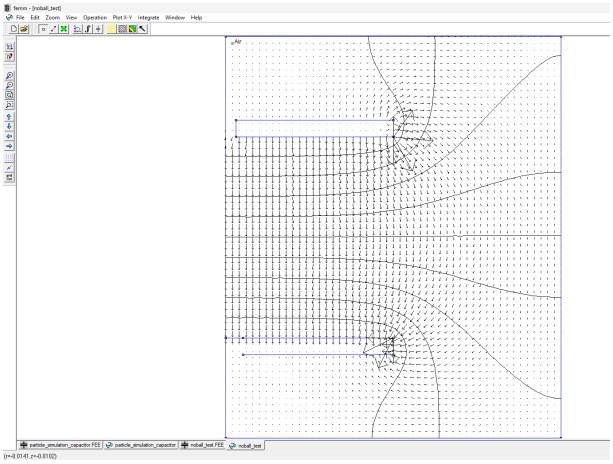

Fig. 2. An equipotential contour and superimposed electric field vector plot from our FEMM simulations. This figure demonstrates the uniform quality of the field within the bounds of the capacitor when using a planar cathode (bottom rectangle).

electron trajectories near the centre.

For the anode, we experimented with changing the diameter of the anode hole, but found relatively insignificant effects on the generated field. A small, roughly $2mm$ diameter hole at the centre of the anode offered minimal field aberration while being more than large enough for consistent particle emission with the planar cathode. We also considered using an anodic mesh to allow for particles to pass through the anode at any point. We ultimately rejected this idea, as it would be more difficult to manufacture for little benefit.

### *B. Runge-Kutta Numerical Simulation*

*1) Theory:* The Runge-Kutta method is an iterative method used to find approximate numerical solutions to ordinary differential equations. The idea is based on taking a weighted average of slopes across an interval in order to estimate the average slope, and therefore net differential along a discrete step in the independent variable. A more complete discussion of the numerical basis of the Runge-Kutta 4 method used in this solver can be found in Section XI-B

*2) Our Model:* Given the electric field from our numerical solver, we have the necessary information to use Newton's Second law to track particle motion. It is important to note that Runge-Kutta 4 applies to first-order differential equations, whereas Newton's second law is a second order differential equation. This most effective solution to this problem is to create a system of two first-order differential equations which we can simultaneously solve to model a particle's motion.

While these two equations would typically break Newton's second law into $\mathbf{a} = \frac{d\mathbf{v}}{dt}$ and $\mathbf{v} = \frac{d\mathbf{r}}{dt}$, the electrons in our capacitor will be moving at relativistic speeds. When accounting for relativistic effects, it is more convenient to create a system of differential equations in momentum and velocity. Newton's second law still takes the form $\mathbf{F} = \frac{d\mathbf{p}}{dt}$, however the relativistic momentum includes the Lorentz factor:

$$\mathbf{F} = \frac{d\mathbf{p}}{dt} = \frac{d}{dt}\frac{m_0\mathbf{v}}{\sqrt{1-\frac{v^2}{c^2}}} \tag{1}$$

Where $m_0\,(kg)$ is the rest mass, $\mathbf{v}\left(\frac{m}{s}\right)$ is the velocity, and the Lorentz factor $\gamma$ is given by:

$$\gamma = \frac{1}{\sqrt{1+\frac{p^2}{m_0^2c^2}}} \tag{2}$$

We will track $r, z, p_r, p_z$ as our state variables, first evolving momentum and then posi-

tion using the following system of first-order differential equations:

$$\frac{dp_r}{dt} = qE_r, \quad \frac{dp_z}{dt} = qE_z \tag{3}$$

$$\frac{dr}{dt} = v_r, \quad \frac{dz}{dt} = v_z. \tag{4}$$

Note that we decompose our vectors into radial and z-axis components to reflect the cylindrical symmetry of our capacitor design. We will obtain our $v_r$ and $v_z$ as:

$$v_r = \frac{p_r}{\gamma m_0}, \quad v_z = \frac{p_z}{\gamma m_0}. \tag{5}$$

*3) Implementation and Results:* We exported the radial field produced from our FEMM simulations, and used it to apply our Runge-Kutta 4 numerical solver to track particle trajectories. Note that we mirror the field output from FEMM, leveraging the cylindrical symmetry of our capacitor design. As such, future visualizations show a cross-section spanning the diameter of the capacitor apparatus, rather than solely the radius.

To cope with the heavy computational demands when simulating numerous particles across thousands of steps, we applied a vectorized code structure to simultaneously evolve the states of all particles. This allowed computing the trajectories of thousands of electrons through $15000$ time steps in just a few seconds on a consumer-grade laptop. In our implementation, we also used a relativistic conservation of energy verification method to validate our results.

When simulating the trajectories of electrons liberated from either of our raised emitter designs, we noticed strong divergence of the beam at the emitter itself. Regardless of the emitter design, the beam began to split from first acceleration, as shown in Figure 3. This resulted in a small portion of the electrons passing through the hole in the anode, and those that did continued to diverge along their linear path.

We noticed that switching our cathode design to a planar cathode practically eliminated all divergence of the beam, as shown in Figure 4.

All particles liberated within the radius of the anode hole would escape the capacitor on an undeflected path, to a good approximation.

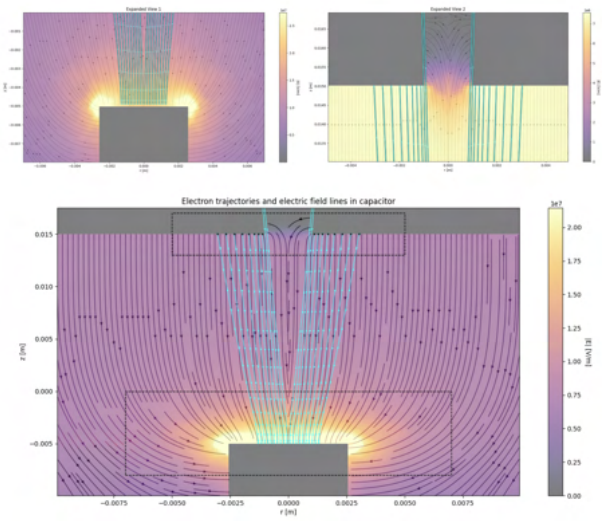


Fig. 3. The simulated blue trajectories lines of electrons liberated from the tip of a squared cathodic emitter (bottom grey rectangle) towards the anode (top grey rectangle). The black lines are a vector plot of the electric field. The coloured heatmap represents the magnitude of the electric field. The bottom figure shows a view of the broader capacitor apparatus, where the plate of the cathode is out of sight. The two expanded views, indicated by rectangles with dashed borders, more clearly show the field divergence around the emitter (top left) and the anodic hole (top right).

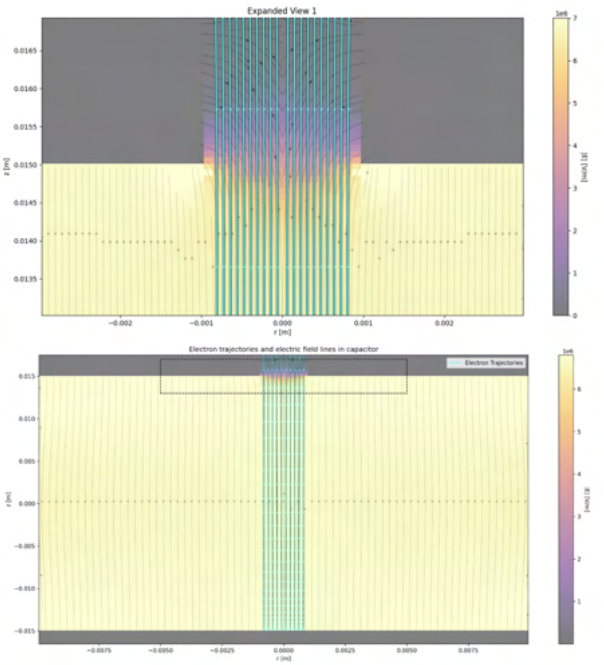


Fig. 4. The simulated trajectories of electrons liberated at a planar cathode. The bottom image shows a full view of the capacitor, while the top image shows the outlined expanded view. In the top image, some divergence of the beam can be shown due to irregularities in the field produced by the hole in the anode plate.

The field aberration at the anode hole was minimal, and by this point the electrons are

travelling quickly enough to be nearly undeflected. This vastly increases the area from which electrons must be liberated in order to get a successful particle emission, and also ensures that particles are emitted in a straight, relatively collimated beam perpendicular to the parallel-plate setup.

Both designs involved electrons traversing the entire potential difference, and therefore gaining maximum energy. We verified this using our relativistic conservation of energy method. However, the planar cathode has the added benefit of being easier to manufacture.

### C. Conclusions

We evaluated how different capacitor geometries would affect the trajectories of electrons as they are fired from the cathode to escape through the anode. Notably, we found that using a flat cathode would allow for the straightest paths when electrons were liberated, and result in almost no divergence of the electron beam. We also found that an anode with a small central hole would consistently allow this collimated beam of electrons to escape.

## III. High Voltage Circuit Design

### A. Circuit Theory

A Cockcroft-Walton voltage multiplier uses a cascading series of stages, each composed of capacitors and diodes, to turn an AC sinusoid into an amplified DC voltage. Namesake physicists John Douglas Cockcroft and Ernest Thomas Sinton Walton first used this circuit to power their own particle accelerator, and as such we find it to be a fitting choice of amplifier.

The voltage multiplier operates by chaining individual stages together, with each stage adding an additional $2V_p$ to the DC output voltage, where $V_p$ is the amplitude of the input AC voltage source. The charging-up of the circuit can be described using a water-pump analogy. Imagine needing to pump water to the top of a well, but the pump can only move water by $1$ meter at a time. Our AC source acts as this pump, where the maximum terminal voltage is $V_p$, its amplitude. The solution to this problem is to pump the water up in stages. First, we can lift up a bucket to $1$ meter above the pump, and offload this water into an adjacent bucket. Then we can use the pump to lift each bucket by an additional $1$ meter – our first bucket lifts water from $0 \rightarrow 1$ meter, while the adjacent bucket lifts water from $1 \rightarrow 2$ meters. We can repeat these stages until the water reaches the top of the well.

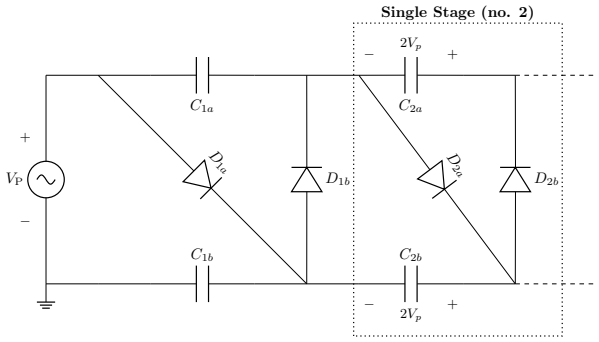


Fig. 5. Circuit diagram for a Cockcroft-Walton voltage multiplier with a single stage enclosed by a dotted box. The circuit forms a ladder-like topology of diodes and capacitors, converting an AC input into a multiplied DC voltage.

In our analogy, the capacitors act as 'buckets' of charge, while the diodes act as one-way valves to prevent the backsliding of charge in our circuit. Each stage consists of two diodes and two capacitors, is self-contained, and can be stacked, ideally infinitely. The ideal output voltage relative to ground, i.e. the voltage of the node at the anode of $D_4$ can be found as:

$$V_{\text{out}} = 2nV_p \tag{6}$$

Where $n$ is the number of stages. In reality, our system has leakage, and our charge pump encounters the accumulating resistance of the wires and diodes. However, this circuit is still incredibly useful, for example in our case, amplifying a $5kV$ sine wave into a $\sim 45kV$ DC potential for our electron diode.

### B. Methods

To generate high voltages to accelerate electrons to high energies, we fed the output of a DC-AC high voltage generator into a Cockcroft-Walton voltage multiplier circuit. The generator converts a $\sim 6V$ battery input into a $\sim 5kV$ peak-to-peak output sine wave. The magnitude of this sine wave limits the DC potential we are able to create using our Cockcroft-Walton circuit. We attempted to further increase its output using a larger

input voltage, but found that the high-power transistor used in the oscillator circuit would burn out.

We used a series of high-breakdown voltage capacitors and diodes to build our Cockcroft-Walton circuit. In testing its output, we found that the driver circuit was able to sustain about seven stages, while adding more gave diminishing returns.

To measure the voltage obtained by our circuit, we used three methods.

The simplest, most imprecise method we used was measuring the maximum arc length producible by our circuit. The breakdown voltage in air is about $30kV/cm$, but this figure is subject to fluctuations in environmental conditions, such as pressure, humidity, and temperature. We primarily used this method to corroborate measurements obtained via other methods.

The second and our most used measurement method was a high-impedance resistor divider, which consisted of two $100G\Omega$ resistors in series with a $2M\Omega$ measurement resistor. A difficulty with measuring high voltages is that they often prefer to behave following quantum, rather than classical rules, in the sense that they behave differently depending on whether they are being measured. Especially in the case of a Cockcroft-Walton multiplier, the circuit will behave drastically differently even under light load compared to no-load conditions. As such, extremely high resistances are necessary to avoid 'voltage sag' due to current through the resistors loading down the circuit. Even corona discharge from the wires in the circuit to the surrounding air accelerates charge leakage, and limits the achievable voltages in the Cockcroft-Walton. We found that using this $1 : 10^5$ ratio of large resistances sufficed, although still impacted the circuit. It is important to note that the multimeter used to measure the voltage across the $2M\Omega$ resistor itself has an impedance of about $10M\Omega$, which must be factored into the conversion ratio. We also tried using an op-amp voltage follower circuit to avoid loading down the measurement with the multimeter, but found no significant advantage.

The third method we used to measure voltage was a specialized high-voltage measurement probe. However, we could not directly measure the voltage of our Cockcroft-Walton output as the probe was only rated for $30kV$. As such, we used it to corroborate the output voltage of only the first stage of the Cockcroft-Walton.

Together, we used agreement between our three measurement methods to find the voltage output from our circuit, i.e. the voltage across our electron diode, which will help us predict the expected electron energies.

### C. Other Elements

We considered both thermionic and photoelectric methods of liberating electrons from the cathode of our apparatus.

In our experiment, we must hold the cathode at a negative potential with respect to the grounded anode. Using thermionic means of electron liberation would require a heating element to also 'float' at this low negative potential. This is accompanied by a host of complexities. If we instead ground the cathode, where electrons are emitted, and hold the anode at a large positive voltage, then upon passing through the anode, electrons would decelerate as they approached any other object, even our measurement device.

Alternatively, using photoelectric methods of emission are as simple as shining a UV light or laser on the plates of sufficient energy to overcome the work function of the metal. This will liberate photoelectrons with negligible kinetic energy and is a suitable choice for our apparatus.

## IV. Apparatus Design

We sought to design an apparatus that would include a fully enclosed housing for the Cockcroft-Walton voltage multiplier, as well as a parallel-plate setup for the diode.

### A. Circuit Housing

Our main considerations when designing the circuit housing were ease of adjustability and high voltage safety.

We require that the Cockcroft-Walton circuit is housed in an isolated environment for high-voltage safety. Our first iteration of the box featured 3D-printed elements as seen in Figure 6,

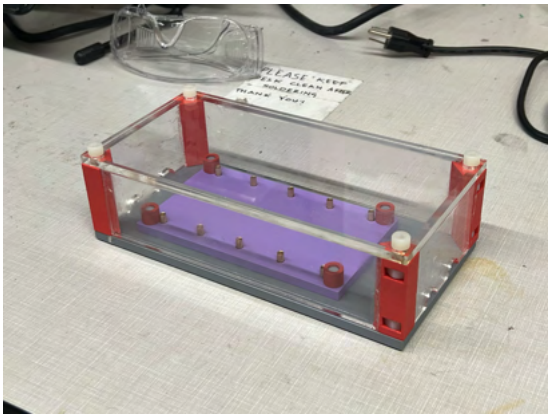

Fig. 6. The first revision of the high-voltage breadboard, featuring 3D-printed components for the corners and base. The assembly comprised of epoxying the walls and the corners together, and screwing the parts together using nut inserts in the corners.

however this resulted in outgassing issues as shown in Section V-C.

We reworked the design to be made out of laser-cut acrylic components and held together using nylon screws as seen in Figure 7.

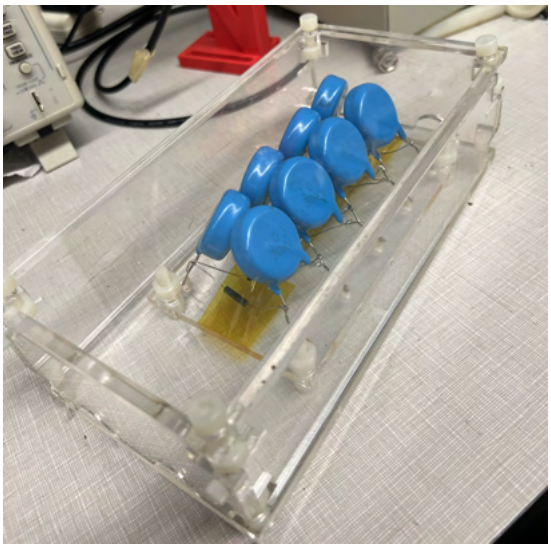

Fig. 7. The second revision of the breadboard, made entirely of acrylic and assembled using nylon screws and tapped drill holes.

Both revisions included a breadboard-style mounting plate for the legs of the components. Bullet connectors were used to neatly contain the soldered connections. The joints use nylon nuts and bolts for assembly.

### B. Diode Stand

Our main considerations when designing the diode were avoiding arcing between the electrodes and their environment.

We first laser cut the electrodes out of aluminium using a fibre laser cutter, with dimensions obtained via our particle simulation in Section II. We affixed our electrodes in the diode device using a screw-down clamping mechanism, which minimally impacted the generated electric field. In future iterations, we replaced the cathode clamping system with a bare piece of copper sheet held down on a post, since the aluminium was rough and would sometimes arc to outgas produced by the acrylic. We ensured that there was sufficient clearance between the parallel plates and supports that would bridge the inter-plate gap. This aimed to stop generated x-rays from ionizing the standoffs, and creating a path for flashover to occur.

We created an electrical connection with the electrodes using an inlay in the electrode clamps and routing a wire under each electrode. The press-fit design of the electrode holders results in firm contact between the plate and the wire.

A UV light source was mounted on the diode, aimed at the cathode, to liberate photoelectrons from the surface.

## V. Voltage Breakdown Calculations

When taking into account the possibility of breakdown in our high-voltage setup, we considered various factors: secondary emission obeying Paschen's Law, field emission obeying Fowler-Nordheim theory, and glow discharge due to outgassing in the vacuum chamber. These considerations shaped the design and revision process for our testing apparatus.

### A. Paschen's Law

*1) Theory:* The breakdown voltage of a gas between two electrodes is described by Paschen's Law:

$$V_B = \frac{Bpd}{\ln\left(Apd\right) - \ln\left(\ln\left(1+\frac{1}{\gamma_{se}}\right)\right)} \tag{7}$$

Where $V_B\,(V)$ is the breakdown voltage, $p\,(Pa)$ is the pressure, $d\,(m)$ is the distance separating the electrodes, and $\gamma_{se}$ is the secondary-electron-emission coefficient. The

semi-empirical coefficients $A$ and $B$ are related to the saturation ionization in the gas at a particular reduced electric field $\frac{\mathbf{E}}{p}$ and the ionization energies of the gas molecules, respectively [1].

At larger values of the product $pd$, above $\sim 10$Torr·cm, the breakdown voltage is roughly linear in $pd$. Of more interest to our application is the behaviour at low $pd$, below the characteristic minimum of the Paschen curve, where the breakdown voltage increases very quickly.

The process of this near-vacuum breakdown is described as follows [1]: In an electric field there are always 'random' electron emissions from the cathode due to cosmic rays and UV rays, or secondary emission due to collisions with loose particles. As these emitted electrons are accelerated, they will sometimes collide with gas atoms, producing a positive ion and more liberated electrons. This positive ion will be accelerated back towards and collide with the cathode, causing additional secondary emission. When this process becomes a self-sustaining cascade, dielectric breakdown occurs.

*2) Methods and Results:* While the exact parameters of Paschen breakdown are dependent on specific experimental conditions, we seek to estimate the required pressure and distance conditions that will avoid breakdown across our diode.

For most metals, the maximum value of $\gamma_{se}$, a material property susceptible to external conditions, typically lies in the low single digits [2]. We can take $\gamma_{se} = 4$ as a conservative estimate for a contaminated Aluminium plate under high vacuum [2].

We then examined literature to find examples that investigate low-pressure Paschen breakdown behaviour. Using empirical material-dependent coefficients extracted from these sources, we plotted Paschen curves for various capacitor plate separations to obtain an estimate of the pressure and distance combination required [1]. One such plot is shown in Figure 8.

To reinforce these results, we examined plots from other sources to cross-check our results. Paschen curves for similar gases offered more forgiving pressure requirements and were consistent lower values of $\gamma_{se} \approx 0.4$ [1].

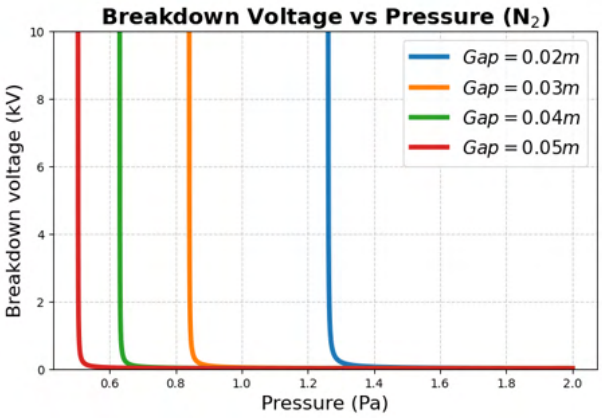


Fig. 8. Paschen curves for various electrode separations using coefficient data obtained from [2]. The $\gamma_{se}$ value is conservatively estimated to be 4. Lower values result in higher breakdown voltages at higher pressures. The vertical spikes indicate the pressure at which the breakdown voltage increases drastically for a given inter-electrode spacing.

Based on these findings, our estimates of the secondary-electron-emission coefficient in our system predict that for a $3cm$ electrode separation, we should not expect Paschen breakdown below $0.5$Pa.

However, these calculations cannot exactly characterize factors such as surface condition and outgassing, which may result in localized environmental fluctuations. The true vacuum limitations of our system must be explored through experimental testing, as discussed in Section VI.

## B. Field Emission

*1) Theory:* The Fowler-Nordheim model describes field emission, in which electrons subject to a strong bias may quantum tunnel through the surface potential barrier of the electrode, becoming a free electron. The application of a large potential difference across a small gap, in the tens of thousands of volts for example, results in an increasingly thin triangular potential barrier at the cathode surface. The tunnel current response is highly non-linear, increasing drastically when conditions surpass a certain threshold [3].

An important factor in evaluating the significance of field emission is the influence of local field enhancements that may occur due to microscopic material defects. The field enhancement factor $\beta$ characterizes this effect, defined as the ratio of locally-enhanced fields

to the macroscopic field in the device. Typical vacuum precautions like polishing surfaces and avoiding sharp corners in design can limit the severity of field enhancement, but there is always an unavoidable presence of defects in a sample that must be considered. The importance of field emission considerations in an electron diode gun is well noted in similar applications, where it is the most limiting factor on allowed accelerating voltages [4].

*2) Methods and Results:* We can use Equation 8 in Section XI-A to plot the breakdown current at different electrode voltages and local field enhancement factors to get a dimensional estimate of the breakdown current and its relative importance [3]. The work function of Aluminium is taken as $\phi = 4.2\,\mathrm{eV}$ and the effective emitter area was calculated assuming a polished 1-inch diameter aluminium cathode. We plot these curves in Figure 9 for various field enhancement factors, with literature estimating $\beta \approx 10 - 100$ for a typical cathode's micro-irregularities [5].

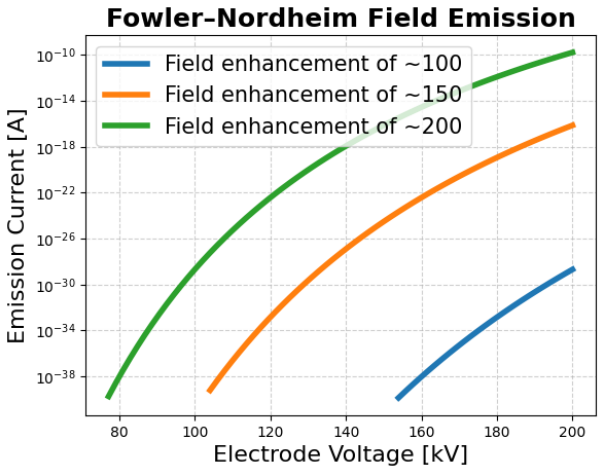


Fig. 9. The Fowler-Nordheim field emission model's breakdown current predictions for various field enhancement factors against electrode voltage. Even conservative estimates of the field enhancement factor and electrode voltage yield negligible currents of well below a nanoamp.

As seen in Figure 9, an estimate for the importance of field emission using parameters comparable to our design conditions shows a negligible contribution to breakdown. As such, we will not take further steps beyond the precautionary design principles described earlier to address field emission.

### C. Vacuum Outgassing

*1) Theory:* Outgassing is the release of trapped vapours or other compounds from components in a vacuum chamber. When drawing a vacuum, these factors can limit achievable pressures, and importantly, can cause breakdown in high voltage systems. Outgassing can increase local pressure around a region, which may lead to the ionization of the gas molecules, inducing breakdown.

*2) Considerations:* Preliminary tests showed localized glow discharge from the electrode or elements of the Cockcroft-Walton voltage multiplier circuit to 3D-printed components used in our first design of the circuit housing and diode stand. During these tests, the measured pressure in the chamber was around $0.1Pa$, which is below our predicted Paschen breakdown threshold. We

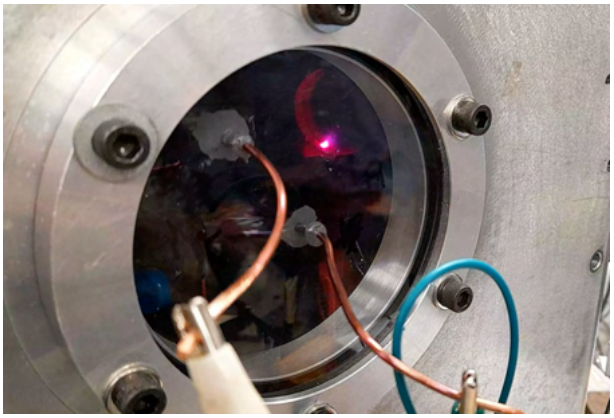

Fig. 10. A reddish-pink arc between the cathode and its 3D-printed mount shows dielectric breakdown due to outgassing of the PLA. We observed this breakdown as a repeated clicking sound accompanied by the coloured flash, primarily around the cathode but also present around the voltage multiplying circuit.

suspect that there was significant outgassing from the 3D-printed PLA components in the diode and circuit assembly. This likely limited the voltage obtainable across the diode, potentially damaged parts of the circuit, and produced disruptive electrical noise on the MiniPIX radiation camera.

Steps we can take to reduce outgassing and its related impacts include replacing high-outgassing components with those redesigned using more optimal materials, removing unused components entirely, and improving the quality of the vacuum.

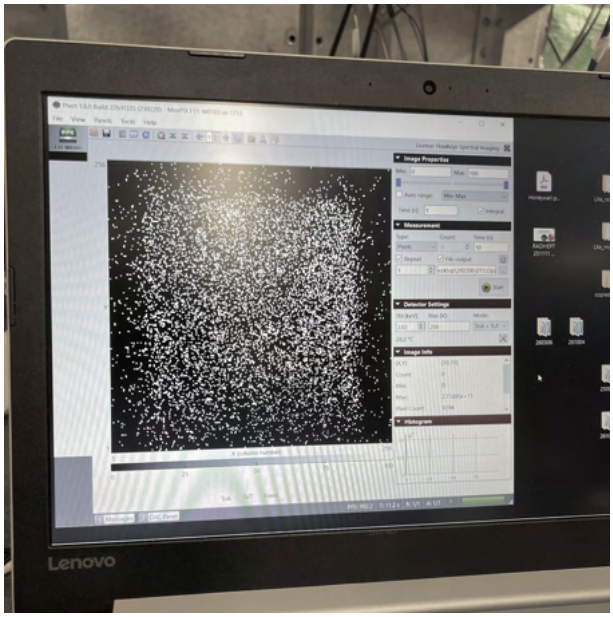


Fig. 11. Electrical interference produced by the outgassing breakdown resulted in static-like noise on the MiniPIX radiation counter, inhibiting analysis of generated particles.

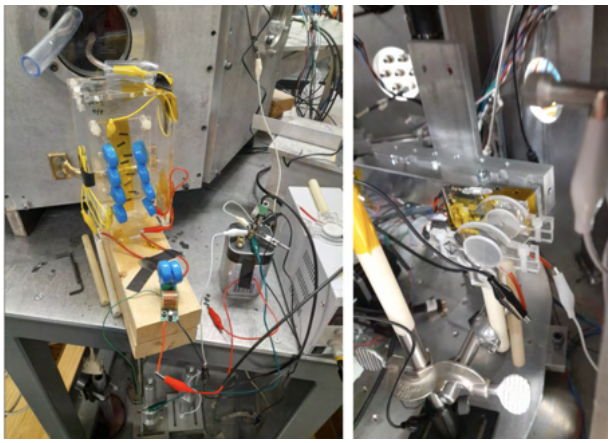

Fig. 12. The modified experimental setup from our preliminary tests. We found more success with the Cockcroft-Walton outside the chamber (left), as it removed potential sources of outgassing and breakdown. The diode inside the vacuum chamber (right) is grounded via the chamber walls, and is aimed at the MiniPIX. We kept this arrangement the same for future tests, albeit with modification to the individual parts.

## VI. Voltage Breakdown Observations

After taking preventative measures and designing our apparatus accordingly, we performed iterative testing and revision. We found breakdown to be the most significant challenge obtaining particle detections.

Our first attempt to mitigate this involved redesigning the apparatus to replace 3D-printed parts with laser-cut acrylic and nylon standoffs. Acrylic outgasses significantly less than PLA, however most plastics experience some unavoidable outgassing. A further measure we took was to evacuate the chamber of as many extraneous items as possible. This included extracting the Cockcroft-Walton circuit outside of the vacuum chamber, and connecting it to the diode via a potted wire through a custom-altered vacuum chamber plate. The new setup can be seen in Figure 12.

This improved, but did not entirely resolve the arcing issues. The wire connected the Cockcroft-Walton circuit outside the chamber to the diode within was arcing to the walls of the vacuum chamber. Additionally, the diode itself was arcing into free space, likely confirming the remaining presence of outgassing from the acrylic stand.

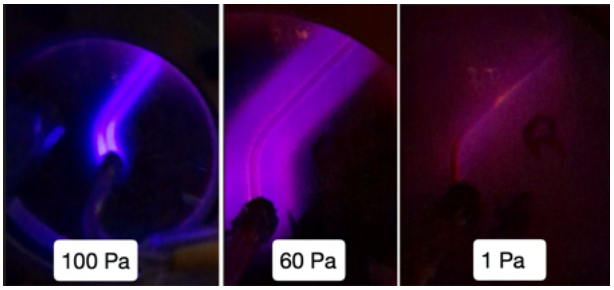


Fig. 13. Glow discharge between the vacuum chamber's metal walls and the high-voltage wire carrying the multiplied Cockcroft-Walton output. The various states of discharge are taken under varying pressure conditions, listed from left to right as $P > 1mbar \approx 100Pa$, $P \approx 0.6mbar \approx 60Pa$, and $P \approx 0.01mbar \approx 1Pa$. At lower pressures, this (pretty!) glow discharge transformed into intermittent arcing, with discharges over one inch in length.

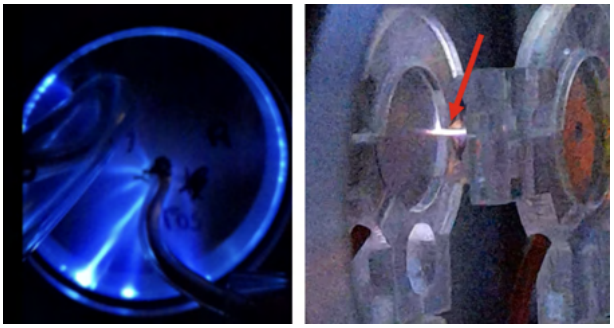

Fig. 14. The input wire to the chamber arcing to the surrounding metal, over one inch away (left). The cathode of the diode arcing into free space, likely due to fine grooves or imperfections in the surface (right). Both occurrences happen at pressures on the order of $0.05Pa$.

We consistently see breakdown at pressures below our $0.5Pa$ estimate for the Paschen limit in our system. Together, we take these

observations to mean that our Paschen breakdown estimates were overly generous. This is most likely attributable to the non-idealities of our apparatus, namely outgassing of materials, imperfections on material surfaces. To further reduce breakdown, we must improve the quality of the vacuum attained.

## VII. Summative Testing

After testing and revising the design, we obtained a prototype for our desired electron diode source. We completed a full test that involved liberating electrons solely via self-emission, as well as with the help of a UV light or laser, and measured the particle production with the MiniPIX radiation detector.

### A. Methods

We assembled the diode inside the vacuum chamber, wiring ground to the chamber housing, and carefully isolating the high-voltage wire through an entry port on one of the walls. The cathode was sanded with 200 grit sandpaper. We ensured the cathode and anode were evenly spaced, parallel, and pointed towards the sensing area of the MiniPIX radiation detector.

We used a red alignment laser and orange fluorescing paper to ensure the UV laser setup directed the beam to the center of the cathode.

We drew the vacuum to below $2.0 \cdot 10^{-5} mbar$, or about $0.0020 Pa$.

Outside the chamber, we connected the battery in series with the high-voltage generator circuit, which we fed into our Cockcroft-Walton multiplier circuit. The output of the voltage multiplier was connected to the high-voltage lead running through the entry point of the vacuum chamber to the diode. We also connected it to our resistor divider in order to measure the diode voltage during our tests.

The simplified circuit diagram for our final test is shown in Figure 17.

The parameters we varied during our experiment were the voltage of the diode, activating the room lights, the UV light, and the UV laser. The laser itself had different power settings that we also varied. Each measurement from the MiniPIX consists of 10 seconds of data collection, in which the detection location, time of detection, and energy of each particle is written to a log file. The particle detector

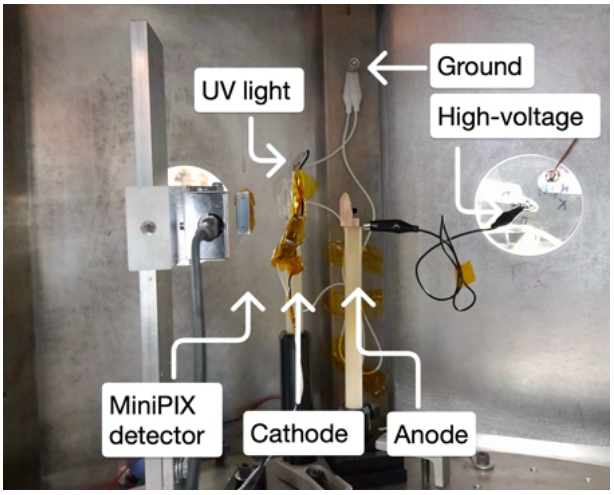


Fig. 15. A side view of the final arrangement of our diode setup. The copper cathode (right post) is connected to the output of our Cockcroft-Walton circuit via the black wire through the clear entry port (right). The anode (middle post) is grounded via the white wire to the chamber wall, and aimed at the MiniPIX detector (left post). The UV light is mounted on the anode, and the laser enters through the left clear entry port.

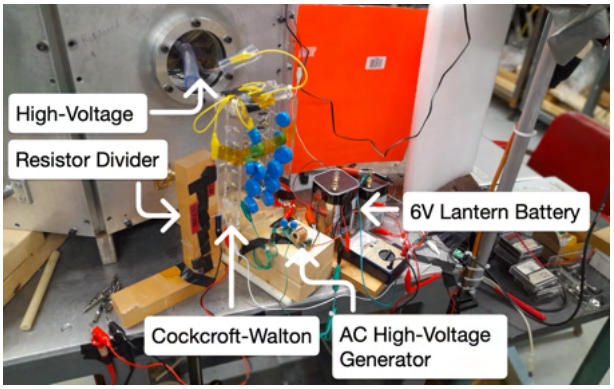


Fig. 16. The final arrangement of our circuit elements outside the vacuum chamber.

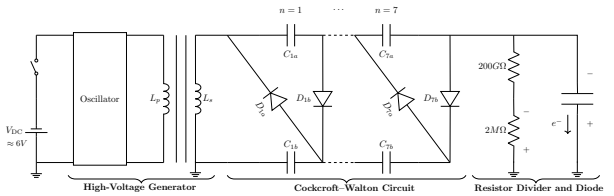


Fig. 17. Circuit diagram of our final testing setup. A large 6V lantern battery was used to power the high-voltage generator circuit. Its AC output was fed into the Cockcroft-Walton voltage multiplier. The output node of our seven-stage ladder is used to hold the diode at a high potential. Note that the diodes are all reversed compared to a canonical Cockcroft-Walton circuit, as we hold the cathode at a large *negative* potential with respect to the grounded anode.

is visualized by lighting up the pixel it was detected on.

First, we collected a series of background measurements, using the MiniPIX to measure particle production with voltage off. Within these background measurements, we toggled the status of the room lights, UV light, and UV laser to understand the background levels of particle detection, and whether they vary with these parameters.

To collect data with the voltage on the diode activated, we charged the diode by repeatedly pulsing the oscillator circuit switch. Once the diode voltage reached a roughly stable maximum, as observed via the resistor divider multimeter reading, we released the switch and started the MiniPIX. We completed a series of $10$ second measurements while the diode voltage decayed, recording the voltage of the diode at the start of each one. The MiniPIX has a $6\mu m$ aluminium foil filter in front of the sensor, which should not allow electrons to pass below $22keV$.

We did not collect data while activating the oscillator circuit to avoid electrical noise from charging the diode contaminating our measurements.

### B. Results

We obtained almost $200$ separate files, each corresponding to a $10$ second measurement from the MiniPIX, from which we can analyse the detection position and energy spread of our particles across our various background and active trials.

First, we can plot a heat map of the location of all particle detections when the diode voltage was active versus when it was inactive. This is shown in Figure 18.

In the background image, we note that there are very few detections. The heat map legend shows that on average, each pixel is active for at most $4\%$ of the trials, which corresponds to once out of the $24$ trials represented. Additionally, the impacts are very sparse. The linear clusters of detections represent cosmic background radiation, specifically muons. Other detections represent different forms of background radiation.

In the charged heat map, we notice a strong cluster of impacts near the centre, with the heat

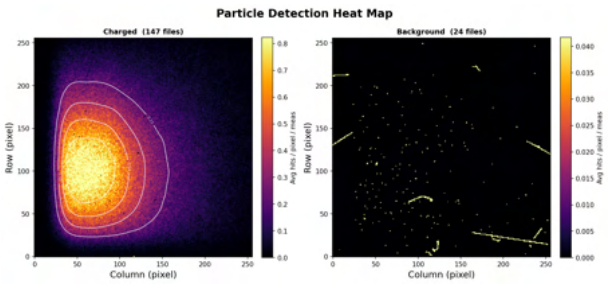


Fig. 18. A heatmap showing the location of particle detections by the MiniPIX radiation detector for trials where the diode is charged (left) and background trials (right). Note that the sensor's mounting frame shields a $\sim$ 20 pixel border around the device, resulting in a square dark band around all detections. Each pixel is assigned a colour that represents the fractional number of trials in which it was active.

map legend showing that the most-hit pixels were active for as many as $80\%$ of the $147$ trials plotted. Despite the clipping of detections at the edges, we have shown annular contour rings that represent lines of equivalent detection frequency. Examining the rings further from the edges, we notice a distinct pattern of concentric circular arcs that reflect the circular opening in our anode. As the rings get larger, our detections get increasingly diffuse, as these detections are increasingly composed of scattered electrons and bremsstrahlung produced when electrons impact the metal anode.

Using the contour lines and comparing to our background results, we can conclude that the diode successfully produces a beam of radiation incident upon the particle detector. The loose distribution of impacts, seen via the separation of adjacent contour lines, indicates that we could improve collimation of the beam, or reduce scattering.

Second, we can examine that particle detection rate against diode voltage for our diode, comparing the various illumination conditions. Our series are shown in Figure 19. Due to the exponential increase in count rates as voltages increase, we use a log plot to visualize the data. We note that for voltages above $\sim 30kV$, increasing the diode voltage linearly increases the log count rate, and therefore exponentially increases particle production. Below $\sim 30kV$, we notice that there is a sharp drop-off and subsequent plateau of count rates. This somewhat agrees with our knowledge that the $6\mu m$ aluminium foil filter on the MiniPIX should result in a cutoff energy around $22kV$.

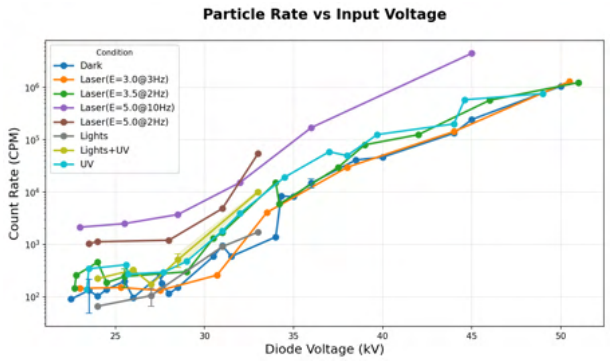


Fig. 19. A log plot showing the particle detection rate against diode voltage. We separate data series by conditions, as given by the legend.

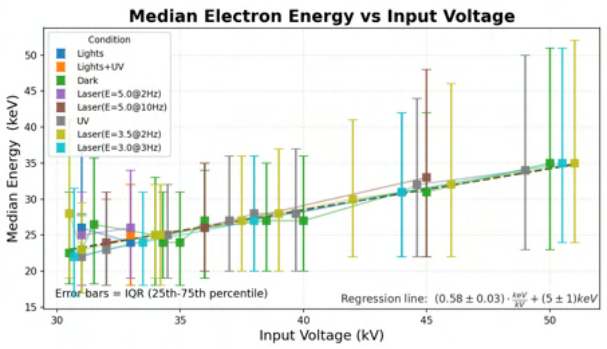


Fig. 20. A scatter plot relating the median energy of detected electrons to voltage across the diode. Our line of best fit was calculated with `scipy.optimize.curvefit`, and has the values $y = (0.58 \pm 0.03)\,\frac{keV}{kV} \cdot x + (5 \pm 1)\,keV$.

We note that the UV laser at a power of $5.0W$ produces roughly an order of magnitude more counts than our no-UV tests with the room lights on or off. The UV light mounted on the anode, for comparison, results in roughly double the count rates over our base test.

However, we also note an exponential increase in emissions with voltage, even if the photocathode power remains constant. This indicates a high rate of self-emission from the cathode, even without photo excitation. While we sanded the cathode, we suspect that the micro-scale surface roughness of the cathode resulted in these high level of self-emission, and contributed to our earlier difficulties preventing breakdown. Together with the exponential relation between voltage and emissions, we conclude that the field enhancement on the surface of the cathode, and perhaps also the secondary emission coefficient, far exceeds our previous estimates.

We can conclude that the UV light source and laser enhance emission. However, due to surface roughness, the cathode has high levels of self emission. To reduce the particle flux, and potentially also increase the allowed pressures at which breakdown does not occur, we must improve the surface condition of the cathode to reduce local field enhancement. This could be done by more carefully manufacturing and polishing our electrodes.

Lastly, we can create a scatter plot comparing the mean detected electron energy against the voltage of the diode. This is shown in Figure 20.

We note that there is a linear increase in median particle energy with diode voltage, as expected. However the fitted slope is only $m = (0.58 \pm 0.03)\,\frac{keV}{kV}$ The ideal slope of our relationship is $1\frac{keV}{kV}$, where doubling the voltage doubles the energy of all produced electrons. In reality, not all electrons that reach the detector have the maximum possible energy. Many go through collisions with gas particles, scatter off of surfaces, or create bremsstrahlung of varying energies, all of which are detected by the MiniPIX. This decreases the median energy of our detected particles, as only the electrons on the high end of our energy spectrum meet our ideal $1:1$ voltage to energy conversion.

We can conclude that increasing the diode voltage linearly increases the voltage of generated electrons. However, due to scattering in our large flux of particles, electromagnetic filtering must be applied to select only the particles of maximum energy, and provide monochromatic electrons for calibration of our detection equipment.

### C. *Improvements*

Given the findings from our analysis, we can devise various improvements that will advance our prototype towards use in calibrating high energy space particle detectors.

We noticed that while our UV sources multiplied particle production, base levels of self-emission from the cathode were very high. To address the high flux of particle production and noisy energy spread due to scattering, we propose three solutions.

The first is simply polishing the cathode surface to reduce field emission, and therefore

the particle flux. Field emission has a highly non-linear relationship with $\beta$, the local field enhancement parameter that relies on micro-scale surface smoothness and material defects. We expect that polishing the surface to high quality smoothness would drastically reduce the particle flux, allowing for more controllable particle generation using our UV methods.

Second, we noted that our detections did not reflect a perfectly collimated beam of electrons, likely due to bremsstrahlung. To address the diffuse scattering of our particles across the detector, we propose adding a thick lead aperture behind the anode, which will absorb the breaking radiation produced by scattered electrons.

Finally, the energies of our particles are widely distributed. To accurately calibrate space particle detectors, we can apply a magnetic spectrometer to select our highest energy particles from the diode source, within a known energy range, and allow them alone to pass.

A second area of focus would be increasing the maximum energies attainable by electrons by increasing our diode voltage. The primary limitation in our Cockcroft-Walton multiplier is the amplitude of our high-voltage AC generator. Building or buying a higher voltage oscillator, for example one with a $15kV$ peak-to-peak amplitude would result in a $105kV$ DC output for our diode, producing $105keV$ electrons. A minor improvement to our multiplier efficiency would be potting and covering the wiring in our Cockcroft-Walton circuit to avoid air breakdown and mitigate corona charge leakage.

## VIII. Conclusion

Our final testing and analysis allow us to conclude that the diode successfully produces a beam of high energy electrons. Increasing the voltage of the diode increase the energy of electrons. Emission rates can be controlled using UV light to produce more electrons via the photoelectric effect.

From our analysis, we identified several improvements to advance our prototype towards accurate calibration of high-energy space particle detectors:

- While the diode successfully produces a semi-collimated radiation beam incident on the particle detector, a thick lead aperture behind the anode could absorb x-rays from scattered electrons, improving collimation.
- A magnetic spectrometer could filter only the highest-energy particles from the diode source.
- Polishing the cathode surface would reduce $\beta$, decrease field emission flux, facilitate accurate particle selection, and raise the breakdown pressure threshold.
- A higher-voltage oscillator driving the Cockcroft-Walton multiplier would increase the maximum attainable electron energies.

## IX. References


[1] A. J. Lichtenberg, *Principles of plasma discharges and materials processing*. Wiley-Interscience, 2005.

[2] H. Bruining and J. De Boer, "Secondary electron emission: Part i. secondary electron emission of metals," *Physica*, vol. 5, no. 1, pp. 17–30, 1938, ISSN: 0031-8914. DOI: https://doi.org/10.1016/S0031-8914(38)80103-8 [Online]. Available: https://www.sciencedirect.com/science/article/pii/S0031891438801038

[3] M. Radmilović-Radjenović, D. Radjenović, B. Stojičić, and B. Radjenović, "The effect of the field emission on the breakdown voltage characteristics of air microdischarges,"

[4] K. Duncan-Chamberlin, "High-voltage testing for a high-current electron gun," 2013.

[5] C. M. Lampert, "Materials and molecular research division and energy and environment division lawrence berkeley laboratory university of california berkeley ca 94720,"


## X. Acknowledgements


I would like to thank my supervisor, Dr. Robert Fedosejevs, for his support throughout the project. Testing this high-voltage project in a vacuum chamber was only possible due to his expertise in high-voltage safety. I would also like to thank my two graduate student mentors, Caleb Guthrie and John Matthew Gjevre, for

their invaluable assistance and advice at each stage of the design process.

# XI. Appendix

## A. Fowler-Nordheim Model

For a direct-current field, we can model Fowler-Nordheim breakdown current as:

$$I_{\text{DC}} = \frac{1.54 \cdot 10^{-6} \exp\left(4.52\phi^{-\frac{1}{2}} \left(\beta E\right)^2 A\right)}{\phi} \exp\left(\frac{-6.53 \cdot 10^9 \phi^{\frac{3}{2}}}{\beta E}\right) \tag{8}$$

Where $\phi\,(eV)$ is the work function of the electrode, $\beta$ is the enhancement factor of the field, $E\left(\frac{V}{m}\right)$ is the electric field, and $A$ is the effective area of the emitter.

## B. Runge-Kutta Numerical Theory

The Runge-Kutta method is applicable to initial value problems (IVPs) of the form:

$$y' = f\,(y, t)\,, \quad y\,(t_0) = y_0 \tag{9}$$

Runge-Kutta 4, a commonly-used implementation of the broader family of Runge-Kutta numerical methods, has local truncation error on the order of $O\,(h^5)$, and an accumulated error of $O\,(h^4)$.

Take an IVP governed by a differential equation conforming to Equation 9. Using a step width of $h$, we first calculate the derivative at the current position:

$$k_{1i} = f\,(y_i, t_i) \tag{10}$$

Then, we step along the independent axis by half the discretized step width and estimate the new dependent value using a linearisation in our first derivative. We calculate the value of the derivative at this point.

$$k_{2i} = f\left(y_i + \frac{h}{2}k_{1i}, t_i + \frac{h}{2}\right) \tag{11}$$

Then, we again step along the independent axis by half the step width, but this time estimate the new height using our second slope. We calculate the value of the derivative at this point.

$$k_{3i} = f\left(y_i + \frac{h}{2}k_{2i}, t_i + \frac{h}{2}\right) \tag{12}$$

Finally, we step the full step width and estimate the height with a linearisation using the third derivative value we calculated. We calculate the value of the derivative at this point.

$$k_{4i} = f\,(y_i + hk_{3i}, t_i + h) \tag{13}$$

Lastly, we take a weighted average of these 4 derivative values, and take the next step along our solution curve to be a linearization using this averaged slope:

$$y_{n+1} = y_n + \frac{h}{6}\left(k_{1i} + 2k_{2i} + 2k_{3i} + k_{4i}\right) \tag{14}$$